

A&A manuscript no.
(will be inserted by hand later)

Your thesaurus codes are:
09 Interstellar medium (ISM), nebulae (09.09.1; 09.10.1; 09.19.2; 13.25.4)

X-ray observations of supernova remnant G54.1+0.3: X-ray spectrum and the discovery of an X-ray jet

F.J. Lu^{1,2}, B. Aschenbach¹, and L.M. Song²

¹ Max-Planck-Institut für Extraterrestrische Physik, D-85740 Garching bei München, Germany

² Laboratory of Cosmic Ray and High Energy Astrophysics, Institute of High Energy Physics, CAS, Beijing 100039, China

Received , ; accepted ,

Abstract. We present in this paper analyses of the *ROSAT* PSPC and *ASCA* SIS and GIS observations of the Crab-like supernova remnant (SNR) G54.1+0.3. Its spectrum obtained by *ROSAT* PSPC favors a power law model with a photon index of $-0.8^{+0.8}_{-2.0}$, absorbed energy flux in 0.1-2.4 keV of 1.0×10^{-12} erg cm⁻² s⁻¹, and absorption column density of $12.3^{+8.0}_{-3.2} \times 10^{21}$ cm⁻². *ASCA* SIS observation shows that its spectrum can also be best fitted with power law model. The fitted parameters are, photon index $-1.9^{+0.1}_{-0.2}$, absorbed energy flux in 0.7-2.1 keV 6.5×10^{-13} erg cm⁻² s⁻¹, and column density $17.9^{+2.8}_{-2.5} \times 10^{21}$ cm⁻². The high absorption column density indicates a distance similar to the radius of the galaxy. The 0.1-2.4 keV X-ray luminosity of G54.1+0.3 is $3.2 \times 10^{33} d_{10}^2$ erg s⁻¹, where d_{10} is the distance in 10 kpc. With an image restoration method we have obtained high spatial resolution X-ray image of the remnant, which clearly shows an X-ray jet pointing to the northeast with a length about 40'' from the center of the nebula. Its X-ray luminosity in 0.1-2.4 keV is about $5.1 \times 10^{32} d_{10}^2$ erg s⁻¹. The X-ray jet is consistent with the radio extension to the northeast in both direction and position. We propose that the X-ray jet is connected with the pulsar assumed to exist in the remnant.

Key words: X-ray: ISM – ISM: supernova remnants – ISM:jet and outflows –ISM: individual: G54.1+0.3

1. Introduction

Radio source G54.1+0.3 was first suggested to be a Crab-like SNR by Reich et al. (1985) for its flat spectral index of $\alpha \sim -0.1 \pm 0.1$, filled-center morphology and significant polarization. This identification to G54.1+0.3 was confirmed by Velusamy & Becker (1988) with high resolution multifrequency observations with the VLA and OSRT. In the high resolution VLA maps, G54.1+0.3 has a filled-center brightness distribution peaks around R.A.(2000) =19:30:30, DEC(2000)=18:52:11 and extends to the northeast and north (Velusamy & Becker 1988). They pointed out that these extensions are reminiscent of the radio jets seen in the

Crab (Velusamy 1984), CTB80 (Angerhofer et al. 1981) and G332.4+0.1 (Roger et al. 1985).

X-rays from G54.1+0.3 was detected by *EINSTEIN* IPC (resolution $\sim 1'$) with a source strength of 0.016 ± 0.004 counts s⁻¹ in the energy band 0.5-4.0 keV (Seward 1989). No extent to the X-ray emission was found, due to both its small angular size ($2.0' \times 1.2'$) (Velusamy & Becker 1988) and its low flux. A power law spectral fitting with energy index of 1.0 gives column density N_H between 5×10^{21} and 1×10^{23} cm⁻², with the best fit value of 3×10^{22} cm⁻², indicating a large distance of this source.

In the paper we present the analyses of *ROSAT* PSPC and *ASCA* GIS and SIS observations of G54.1+0.3. We obtain its spectral information, and, with the aid of an image restoration method, we obtain a high spatial resolution X-ray map of the remnant which clearly shows an X-ray jet pointing to the northeast.

2. Observations and analysis method

The *ROSAT* PSPC pointing observation of SNR G54.1+0.3 was carried out from April 11th to 18th, 1991 with a total acceptable observational time of 20271 seconds. We use *EXSAS* (Zimmermann et al. 1998) to analyze its spectrum and produce a 0.1-2.5 keV X-ray image (figure 1) whose spatial resolution is the intrinsic resolution of PSPC (40'').

G54.1+0.3 was also observed with *ASCA* observatory (Tanaka et al. 1994) continuously from April 27th to 28th, 1997, using the two Gas Imaging Spectrometers (GIS-2 and GIS-3) and the two Solid State Imaging Spectrometers (SIS-0 and SIS-1). Data were collected by the two GIS detectors with a photon time-of-arrival resolution of 4.88×10^{-4} s in the high bit-rate modes. An effective exposure time 16.5 ks was achieved for each detector. The SIS detectors were operated in the 1-CCD faint mode in which read-out is every 4 s. All SIS data were filtered using the standard screening criteria, which resulted in effective exposures of 19 ks and 20.7 ks for SIS-0 and SIS-1 respectively. Since the two GIS detectors were operated in the high time-of-arrival resolution model, we used the GIS data for temporal analysis. The SIS detectors which are sensitive to photons in 0.5-10.0 keV have superior energy res-

olution compared to the GIS, and so the SIS data are used for spectral analysis.

Due to the small angular size ($120'' \times 75''$) of G54.1+0.3 and the limited spatial resolution ($\sim 40''$) of PSPC, the PSPC observation can not directly give even a coarsely resolved image of G54.1+0.3. In order to obtain an image with higher spatial resolution, we use the widely used Lucy-Richardson formula (Richardson 1972, Lucy 1974) to eliminate the point spread function effect in figure 1. In the iteration process we have used the mean background as the lower limit constraints, in order to improve the quality of the restored image, as done by Li & Wu (1994), Lu et al. (1996) and Zhang et al. (1998).

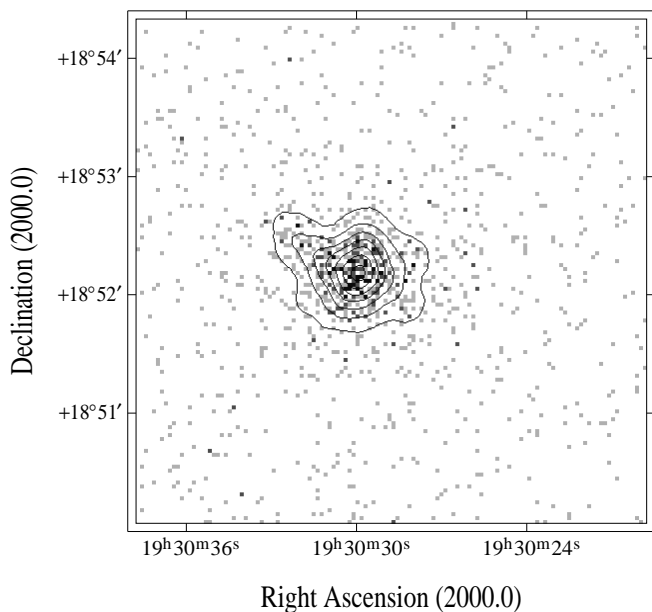


Fig. 1. Count-rate map in 0.1-2.5 keV obtained by *ROSAT* PSPC observation to G54.1+0.3. North is up and east is left. The contours overlaid represent the smoothed count-rate map with a $10''$ FWHM Gaussian filter. The contour intervals are linear in step of 10^{-5} count s^{-1} per $2'' \times 2''$ pixel. The lowest contour corresponds to a brightness level of 10^{-5} cnt s^{-1} per pixel.

3. Results

3.1. Spectrum from *ROSAT* PSPC observation

The *ROSAT* PSPC spectrum of G54.1+0.3 shows a lack of low energy photons and peaks at energy channel 150 (about 1.5 keV). The spectrum can be fitted with power law model and Raymond-Smith (1977) thermal plasma model. The power law model yields a photon index of -0.8 with 1σ error range of -2.8 to 0.0 and an absorption column density of 12.3×10^{21} cm^{-2} with 1σ error range of 8 to 20×10^{21} cm^{-2} (see figure 2). The thermal plasma model derives a plasma temperature of 1.8 keV (> 1.2 keV) and absorption column density of 21.1×10^{21} cm^{-2} with 1σ error range of 15 - 26×10^{21} cm^{-2} . The reduced χ^2 values are almost the same, 0.831 for power law model and 0.834

for thermal plasma model. We adopt the power law model in this paper for it gives the best and the most reasonable fit to the *ASCA* SIS spectrum, as shown in the next section. It gives the absorbed and unabsorbed 0.1-2.4 keV X-ray energy fluxes of 1.0×10^{-12} and 3.4×10^{-12} $erg\ cm^{-2}\ s^{-1}$, respectively. Figure 3 shows the power law model fitting results.

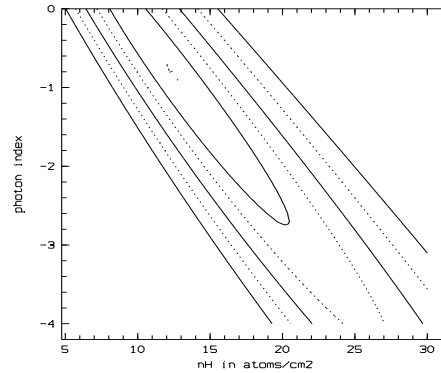


Fig. 2. χ^2 distribution on the column density–photon index plan of the power law spectral fitting of *ROSAT* PSPC observation of G54.1+0.3. Contours from the inner to the outer correspond to 1σ to 5σ .

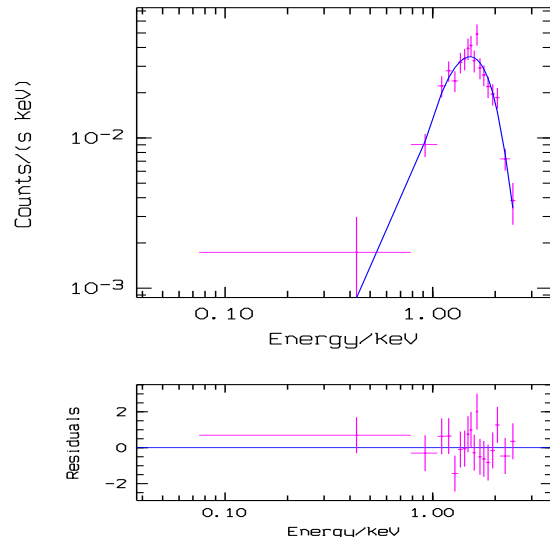


Fig. 3. Spectral fitting results to the X-ray emission of G54.1+0.3 obtained by *ROSAT* PSPC with a power law model. The parameters are presented in the text.

3.2. Spectrum from *ASCA* SIS observation

The SIS spectra of the source were extracted within a 4.5 arcminutes radius region. After subtracted the source region, another region of the CCD was used for background subtraction. The source and background spectra obtained from both SISs were added to obtain improved statistics. The spectral analyses

software is XSPEC. Energies above 8 keV were not used because of the poor signal to noise ratio. We have used power law, blackbody, single temperature bremsstrahlung and Raymond-Smith thermal plasma models to fit the spectrum, and found that only the power law model and the thermal bremsstrahlung model give acceptable and reasonable fits. The obtained parameters of the power law model are: photon index $\alpha -1.9^{+0.2}_{-0.2}$, column density $N_H 17.9^{+2.8}_{-2.5} \times 10^{21} \text{ cm}^{-2}$, 0.7-2.1 keV energy flux $6.5 \times 10^{-13} \text{ erg cm}^{-2} \text{ s}^{-1}$, reduced $\chi^2 0.7$. Parameters of a thermal bremsstrahlung model are: temperature $T_e 7.9^{+3.9}_{-3.1} \text{ keV}$, column density $N_H 15.4^{+2.0}_{-1.9} \times 10^{21} \text{ cm}^{-2}$, 0.7-2.1 keV energy flux $8.6 \times 10^{-13} \text{ erg cm}^{-2} \text{ s}^{-1}$, reduced $\chi^2 0.8$. We choose the power law model in this paper for that it has the smallest χ^2 and a power law X-ray spectrum is the typical property of the X-ray emission of a Crab-like SNR. For illustration, we show in figure 4 the best fit power law model and its residuals.

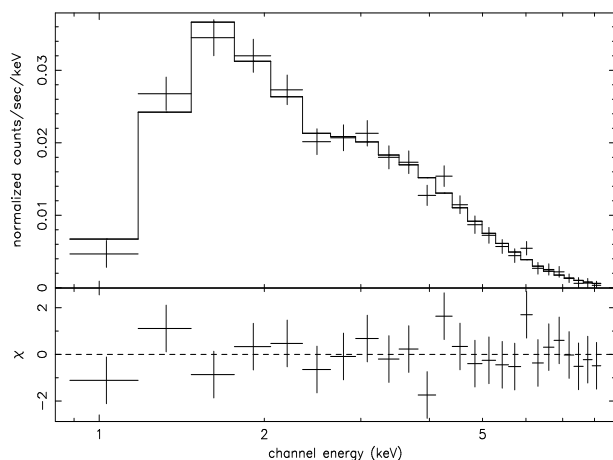


Fig. 4. Spectral fitting results to the X-ray emission of G54.1+0.3 obtained by *ASCA* SIS with a power law model. The parameters are presented in the text.

3.3. Temporal analysis

We examined the *ASCA* GIS data for temporal variability by extracting photons from a 6 arcminutes radius circle centered on the source. A search for coherent pulsations from the source was made by combing the two GIS high-time-resolution data sets (time resolution $4.88 \times 10^{-4} \text{ s}$) and the arrival times of the used 1805 photons were barycentered. We performed a restricted search for periodic signals between 0.01 s and 2 s using a folding technique (20 phase bins per fold), and detected no pulsation with a significance of more than 3σ in this period range.

3.4. Image restoration results

The distribution of photons detected by *ROSAT* PSPC peak at 1.5 keV and is quite symmetric. We thus use the PSPC point spread function in 1.5 keV and the method described in section

2 to restore the original image (figure 1). The iteration stops after 50 iterations (indeed the restored image is insensitive to the iteration number after 20 iterations). The restored image is shown in figure 5, in which a jet-like feature (hereafter JLF) pointing to the northeast appears, in addition to the $\sim 30''$ diameter bright nebula coinciding with the brightest radio region. The angular distance from the head of the JLF to the center of the central bright nebula is about $40''$. The total photon flux of the bright nebula is $2.07 \times 10^{-2} \text{ counts s}^{-1}$, that of the JLF is about $3.9 \times 10^{-3} \text{ counts s}^{-1}$, about 430 and 80 photons have been detected from the bright nebula and JLF respectively.

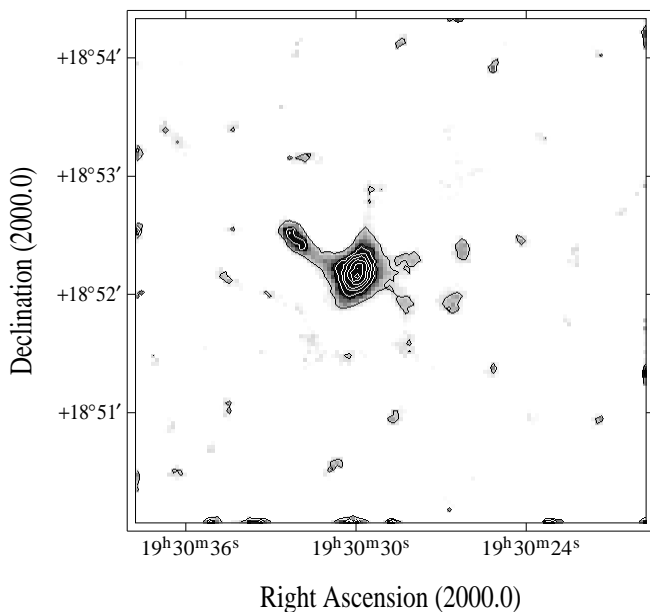


Fig. 5. Restored 0.1-2.5 keV X-ray intensity map of G54.1+0.3. North is up and east is left. The contour intervals are linear with a step size of $4 \times 10^{-5} \text{ cnt s}^{-1}$ per $2'' \times 2''$ pixel. The lowest contour corresponds to a brightness level of $2 \times 10^{-5} \text{ cnt s}^{-1}$ per pixel.

In order to exam the reliability of the restored image, we have performed a Monte-Carlo simulation. Figure 6(a) displays an object similar to G54.1+0.3 in figure 4 in shape and flux. Figure 6(b) is the simulated *ROSAT* PSPC observational result with the same observing time and background level as the real observation to G54.1+0.3, and figure 6(c) is the smoothed image from 6(b). Figure 6(d) is the restored image of 6(b). The simulation shows that the high resolution X-ray image of G54.1+0.3 we obtained is reliable.

4. Discussions

4.1. Distance and X-ray luminosity of G54.1+0.3

Velusamy & Becker (1988) suggested that G54.1+0.3 may have a distance of about 3.2 kpc, if its progenitor is in the star-forming region G53.9+0.3. The galactic HI column density in this direction is about $14.5 \times 10^{21} \text{ cm}^{-2}$ (Dickey & Lockman 1990). The best fit column density we get from *ROSAT* PSPC

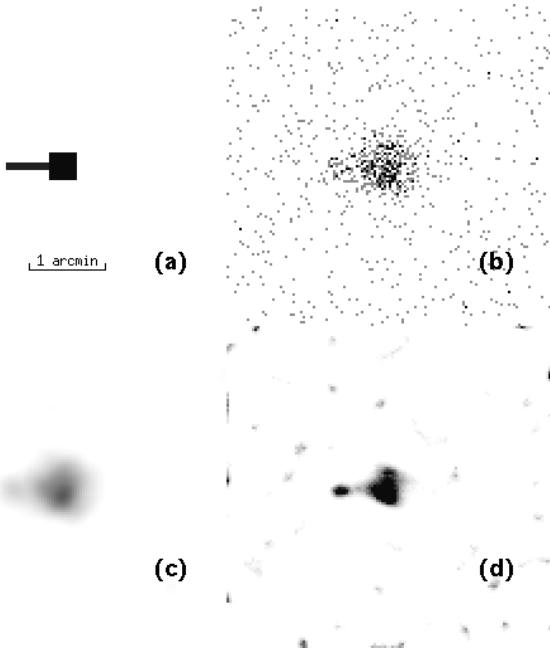


Fig. 6. Simulation of the *ROSAT* PSPC observation and image restoration to an object similar to G54.1+0.3. (a) Object which has a similar shape and the same flux with G54.1+0.3. (b) Simulated *ROSAT* PSPC observation results with the same intergrated time and background level. (c) A smoothed image from (b) and an $10''$ FWHM Gaussian filter. (d) The restored image. Each of the four images has the similar angular size with figures 1 and 4. Note that noisy features have not been displayed in (c) because of a high cut level.

observation is a little lower and the best fit column density of the *ASCA* SIS observation is a little higher than that value. These column densities imply a distance comparable with the radius of the galaxy, similar to the result of *EINSTEIN* IPC (Seward 1989), 3.2 kpc might be then too close and 10 kpc should be a reasonable estimation. The X-ray luminosity in 0.1-2.4 keV is $L_X = 3.2 \times 10^{33} d_{10}^2 \text{ erg s}^{-1}$, where d_{10} is the distance to G54.1+0.3 in unit of 10 kpc. If the distance does not deviate from 10 kpc very much, its X-ray luminosity is three or four orders' lower than Crab Nebula (Helfand & Becker 1987), lies in the lower end of Crab-like SNRs, similar to that of SNR 3C58 (Helfand & Becker 1987; Helfand et al. 1995).

The radio luminosity of G54.1+0.3 is about $5 \times 10^{33} d_{10}^2 \text{ erg s}^{-1}$, derived from the radio observations of Velusamy & Becker (1988). The ratio $L_x/L_r = 0.6$, also similar to that of 3C58 (Helfand & Becker 1987).

Seward & Wang (1988) found that a relation between the X-ray luminosity (L_X) of a plerionic SNR and the spin-down luminosity (\dot{E}) of the central pulsar. Using that relation we can derive $\dot{E} \sim 8 \times 10^{35} \text{ erg s}^{-1}$ for the central pulsar in G54.1+0.3.

4.2. Electron energy distribution

The *ROSAT* PSPC observation of G54.1+0.3 shows that the X-ray flux at 1 keV is about $6.4 \times 10^{-4} \text{ mJy}$. As the radio flux

at 1.4 GHz is 478 mJy, the flux index between radio and X-ray is about -0.7, a little flatter than the *ASCA* SIS obtained X-ray energy index (-0.9) and much steeper than that of radio spectral index (-0.13) (Velusamy & Becker 1998), indicating that the spectrum contains a break between radio and X-ray. Comparing the radio to X-ray flux index, radio flux index and the X-ray flux index, we find that the break is around 10^{11} Hz .

If the relativistic electrons have a power law energy distribution $n_e = E^\gamma$, the spectral index α is $\frac{\gamma+1}{2}$. The spectral break in the spectral means a similar break in the electron energy distribution. The critical radiation frequency of a relativistic electron with energy E in a magnetic field with strength B is $\nu_c = 16.1 B E^2 \sin\psi \text{ MHz}$, where B is in μG , E is in GeV and ψ the incident angle of electron (Lang 1998). The electrons whose maximum radiations are at 1 GHz have typical energies of $9.4 B^{-0.5} \text{ GeV}$ with B the magnetic field strength in μG , assuming that the incident angle is 45° . Similarly the X-ray (around 1 keV) emitting relativistic electrons will have typical energies of $94 B^{-0.5} \text{ TeV}$. If the magnetic field is about $10 \mu\text{G}$, the above estimations show that the electron energy distribution is $\sim E^{-1.3}$ around 30 GeV and $\sim E^{-2.8}$ around 300 TeV. An index break exists between 30 GeV and 300 TeV, probably around 300 GeV.

The life time of a relativistic electron can be represented by $t_{1/2}$, the time of the electron loses half of its initial energy E_0 , $t_{1/2} = \frac{8.35 \times 10^9}{(B \sin\psi)^2 E_0} \text{ years}$, where B is in μG , E_0 is in GeV and ψ the incident angle of the electron (Lang 1998). The lifetimes for the 30 GeV, 300 GeV and 300 TeV photons in $10 \mu\text{G}$ magnetic field are about 5.6×10^6 , 5.6×10^5 , 5.6×10^2 years, respectively. These three typical lifetimes will be used in the discussions of the origin of the electron energy distribution index break in the next paragraph.

If the electrons from the center pulsar have a continuous power law energy distribution initially, the observed break should be due to the short lifetime of the high energy electrons. Because the low energy electrons which radiate radio emission have a long lifetime, their energy distribution represents the initial electron energy distribution well. The initial energy flux ratio $\frac{f_{1.4\text{GHz}}}{f_{1\text{keV}}}$ is then 11.75. The currently observed energy flux ratio $\frac{f_{1.4\text{GHz}}}{f_{1\text{keV}}}$ is 7.8×10^5 , indicates that the age of G54.1+0.3 would be at least $\frac{7.8 \times 10^5}{11.75} \times 5.6 \times 10^2 = 3.7 \times 10^7$ years. This large age value shows that the observed electron energy distribution break is quite probably an intrinsic property of the electrons from the central pulsar.

4.3. X-ray jet

For the first time an well resolved X-ray image of G54.1+0.3 has been obtained. It shows a JLF pointing to the northeast. The simulation shows that such a structure can be clearly resolved by *ROSAT* PSPC with the aid of an image restoration technique. The simulation also shows that this feature can not be attributed as the fluctuations of the bright source, it is an intrinsic structure of the object.

We have studied the possibility that the JLF is indeed a separate object lies in a similar direction with G54.1+0.3. We find that there is no identified object in the 30'' vicinity of the JLF except G54.1+0.3. The optical plate obtained by Palomar Observatory Sky Survey and electronically reproduced by Skyview of NASA/GSFC shows no source in the JLF region too. The JLF shown in figure 5 shows some enhancements in the head. But it might be a false phenomenon caused by the low quality of the original data and the restoration process, as can be found in the simulation, although some similar structures exist in the 4.8 GHz radio map. More simulations show that the length of the JLF is quite reliable, the width of the JLF might have an uncertainty up to $\sim 50\%$.

We have compared figure 4 with the 4.8 GHz VLA map obtained by Velusamy & Becker (1988) in details. The brightest point of the extended X-ray source locates at R.A.(2000)=19:30:30.0, DEC(2000)=18:52:07, which coincides with the brightest region of the radio source. The head of the JLF has a coordinate of R.A.(2000)=19:30:32.2, DEC(2000)=18:52:31, which also coincides with the northeastern enhancement in the radio map. The nice position coincidence of the X-ray and radio sources strongly favor their same origin. However, the X-ray source has a smaller extent than the radio source and no significant X-ray emission has been detected along the northward feature, which was suggested to be the most probable radio JLF by Velusamy & Becker (1988). It might be due to the intrinsic deficiency or the limited sensitivity of the present observation.

There are two possible ways to explain the origin of the X-ray JLF. One is that it is a fragment produced in the supernova explosion, like the fragments detected around the Vela SNR, especially its 'bullet'-like fragment A. (Aschenbach et al. 1995; Strom et al. 1995). However, significant radio emission has only been detected around the head of the fragments, implies that most of the relativistic electrons are in the leading edge of the fragments, close to the shock front (Strom et al. 1995). But in the case of G54.1+0.3 the radio emission has a similar distribution with the X-ray JLF, indicating a similar distribution of relativistic electrons with the X-ray brightness. It makes the fragment origin of the X-ray JLF implausible. The second is that the X-ray JLF is due to the relativistic electrons produced by the central pulsar, like X-ray jets detected in PSR 1929+10 (Wang et al. 1993), Crab SNR (Hester et al. 1995), Vela pulsar (Markwardt & Ögelman 1995), SNR MSH 15-52 (Tamura et al. 1996), SNR CTB80 (Wang & Seward 1984; Safi-Harb et al. 1995) in the galaxy and SNR N157B in the Large Magellanic Cloud (Wang & Gotthelf 1998). The coincidence of radio and X-ray emission in the case of Vela pulsar jet (Frail et al. 1997) and that of SNR N157B (Wang & Gotthelf 1998) strongly support this scenario. We conclude that the JLF we discovered is quite probably an X-ray jet connected with the pulsar in G54.1+0.3.

The X-ray emission of Vela pulsar jet can be fitted with both power law and thermal plasma model (Markwardt & Ögelman 1995), and the X-ray pulsar jet in MSH15-52 appears to be nonthermal. It is difficult to get the spectral properties of the

X-ray jet in G54.1+0.3 with the present data. We assume that it share the same power law model with the whole remnant, and is due to the synchrotron radiation of relativistic electrons from the pulsar. The X-ray luminosity of the jet in 0.1-2.4 keV is then about $5.1 \times 10^{32} d_{10}^2 \text{ erg s}^{-1}$.

From the radio map of Velusamy & Becker (1988) we estimate that the flux of the jet at 4.8 GHz is about 40 mJy. Its X-ray flux at 1 keV is about 9.4×10^{-5} mJy. The two fluxes give a spectral index from radio to X-ray of about -0.73, quite similar to that of the whole remnant. As no significant radio spectral variation across the source has been detected (Velusamy & Becker 1988), the jet electrons have a break with the energy distribution too, similar to the whole remnant.

The distance of the jet head to the nebula center is about 40''. It corresponds to 2 pc if the SNR is 10 kpc away. Recent distance measurements to Vela SNR obtained a distance of 250 ± 30 pc (Cha et al. 1999). If so the Vela pulsar jet is about 3 pc long (Cha et al. 1999, Markwardt & Ögelman 1995). The lengths of the two jets are quite similar.

5. Summary

ROSAT PSPC and *ASCA* observations of G54.1+0.3 imply a large distance comparable with the galactic radius. Its X-ray spectrum is of nonthermal origin. The comparison of the radio and X-ray emissions shows that the energy distribution of the relativistic electrons has a break around 300 GeV. This break is quite probably an intrinsic property of the relativistic electrons from the central pulsar instead of due to the energy loss in the synchrotron radiation process, if G54.1+0.3 is not as old as 3.7×10^7 years.

A high spatially resolved image shows an X-ray jet pointing to the northeast, similar to the radio structures. Its nonthermal spectrum and the existence of X-ray jet confirm the formal identification of G54.1+0.3 as a Crab-like SNR, though no pulsation has been found in the X-ray observation. Future deep X-ray observations with high spatial resolution and spectral resolution telescopes such as Chandra and XMM are invaluable to find out the spectral and spatial structure of the remnant as well as the X-ray jet.

Acknowledgements. F.J. Lu is supported by the exchange program between Max-Planck Society and Chinese Academy of Sciences. He thanks Professor J. Trümper for hospitality. The authors thank Drs S.D. Mao and Q.D. Wang for helpful discussions. This research is partially supported by the National Natural Science Foundation of China and the Special Funds for Major State Basic Research Projects. It has made use of the SIMBAD database, operated at CDS, Strasbourg, France and the Digitized Sky Survey operated by Skyview of NASA/GSFC.

References

- Angerhofer P.E., Strom R.G., Velusamy T., Kundu M.R., 1981, *A&A* 94, 313
- Aschenbach B., Egger R., Trümper J., 1995, *Nat* 373, 587
- Cha A.N., Sembach K.R., Danks A.C., 1999, *ApJ* 515, L25

- Dickey J.M., Lockmann F.J., 1990, ARA&A 28, 215
Frail D.A., Bietenholz M.F., Markwardt C.B., Ögelman H., 1997, ApJ 475, 224
Helfand D.J., Becker R.H., 1987, ApJ 314, 203
Helfand D.J., Becker R.H., White R.L., 1995, ApJ 453, 741
Hester J.J. et al., 1995, ApJ 448, 240
Lang K.R., 1998, *Astrophysical Formulae* (Springer)
Li T.P., Wu M., 1994, Ap&SS 215, 213
Lu F.J., Li T.P., Sun X.J., Wu M., Page C.G., 1996, A&AS 115, 395
Lucy L., 1974, AJ 79, 745
Markwardt C.B., Ögelman H., 1995, Nat 375, 40
Raymond J.C., Smith B.W., 1977, ApJS 35, 419
Reich W., Fürst E., Altenhoff W.J., Reich P., Junkes N., 1985, A&A 151, L10
Richardson B.M., 1972 J. Opt. SOc. Am. 62, 55
Roger R.S., Milne D.K., Kesteven M.J., Haynes R.F., Wellington, K.J., 1985, Nat 316, 44
Safi-Harb S., Ögelman H., Finley J.P., 1995, ApJ 439, 722
Seward F.D., 1989, AJ 97, 481
Seward F.D., Wang Z.R., 1988, ApJ 332, 199
Strom R., Johnston H.M., Verbunt F., Aschenbach B., 1995, Nat 373, 590
Tamura K., Kawai N., Yoshida A., Brinkmann W., 1996, PASJ 48, L33
Tanaka Y., Inoue H., Holt S.S., 1994, PASJ 46, L37
Velusamy T., 1984, Nat 308, 15
Velusamy T., Becker R.H., 1988, AJ 95, 1162
Wang Q.D., Gotthelf E.V., 1998, ApJ 494, 623
Wang Q.D., Li Z.Y., Begelman M.C., 1993, Nat 364, 127
Wang Z.R., Seward F.D., 1984, ApJ 285, 607
Zhang S., Li T.P., Wu M., 1998, A&A 340, 62
Zimmermann U., Boese G., Becker W., Belloni T., Döbereiner S., Izzo C., Kahabka P., Schwentker O. 1998, *EXSAS user's guide*, MPE Report